Published in : Journal of Physics : B Atomic Molecular & Optical Physics (2012), vol. 45, 115101.
Status : Postprint (Author's version)

The spectroscopy of the geminal ethylene difluoride (1,1-$C_2H_2F_2$): the HeI, threshold and constant ion state photoelectron spectroscopies

R Locht[1], D Dehareng[2] and B Leyh[1]

[1] *Molecular Dynamics Laboratory, Department of Chemistry, Building B6c, University of Liège, Sart-Tilman, B-4000 Liège 1, Belgium*

[2] *Center for Proteine Engeneering, Department of Life Sciences, Building B6a, University of Liège, Sart-Tilman, B-4000 Liège 1, Belgium*

Abstract

The threshold photoelectron spectrum (TPES) and the constant ion state (CIS) spectra of the individual ionic states of 1,1-$C_2H_2F_2$ have been recorded using synchrotron radiation. The TPES has been measured between 9.5 and 28 eV photon energy. For comparison, the HeI photoelectron spectrum (HeI-PES) has also been measured and analysed in detail. Numerous vibrational structures, reported for the first time, observed in the ground state and the seven excited states of the cation are analysed. Quantum chemical calculations have been performed and provided support to the assignments. The exceptional contribution of autoionization to the HeI-PES could be emphasized. State-selected CIS spectra highlighted the importance of the autoionizing contribution to the production of almost all ionized states of 1,1-$C_2H_2F_2$ observed in this work. Several peculiarities of the vibrationally resolved CIS spectra are analysed.

(Some figures may appear in colour only in the online journal)

1. Introduction

To the best of our knowledge, the latest and best resolved HeI photoelectron spectrum (HeI-PES) of the geminal difluoroethylene (1,1-$C_2H_2F_2$) molecule has been reported in 1970 by Lake and Thompson [1]. These authors measured adiabatic and vertical ionization energies (IEs) and analysed and assigned the vibrational structure observed in most of the bands.

The photoelectron spectroscopic work has been extended considerably in energy by the use of the HeII resonance line at 30.4 nm (40.8 eV). This provided information on the binding energy of the inner-valence shell orbitals of the molecule. This technique was applied extensively by Bieri *et al* [2, 3] to the investigation of numerous organic fluorocompounds. These authors presented the first HeII-PES of 1,1-$C_2H_2F_2$ and were the first to assign electronic terms to the successively observed bands on the basis of quantum chemistry calculations. Semiempirical, HAM/3 and the many-body Green functional calculations were used.

Several other theoretical investigations were devoted to the description of the halogenated derivatives of ethylene and more particularly to the fluoroethylenes. Heaton and El-Talbi [4] reported *ab initio* molecular orbital (MO) calculations within the Hartree-Fock self-consistent field frame. These authors correlated the MOs to the experimental PES bands on the basis of the correspondence of respective energies.

More recently, Pradie and Linnert [5] reconsidered the IEs of fluorinated ethylenes by *ab initio* calculations. Only the vertical and adiabatic IEs corresponding to the ionic ground state were considered in this paper. Calculations were carried out using the 98 and 03 versions of the Gaussian program packages. Energies were obtained using G2 and G3 theories.

The ionization of 1,1-$C_2H_2F_2$ has also been investigated by photoionization mass spectrometry (PIMS). In their report, Reinke *et al* [6] described the photoionization of the vinylchloride, vinylfluoride and 1,1-difluoroethylene using synchrotron radiation. They investigated in detail both the ionization and the fragmentation of these three molecules.

In an extensive work on the PIMS of 27 fluorinated, chlorinated and mixed halogenated derivatives of ethylene, Kaufel [7] presented a detailed description of the photoionization and fragmentation of 1,1-$C_2H_2F_2$.

Numerous energetic and thermochemical quantities were determined for almost all observed species.

We recently published detailed results on the photoelectron spectroscopic investigation of C_2H_3F between 9 and 21.22 eV by HeI-PES and between 9 and 35 eV photon energy by threshold photoelectron (TPES) and constant ion state (CIS) spectroscopy using synchrotron radiation [8]. With the exception of ethylene iodide, we completed by this way the detailed investigation of the ethylene monohalides by PES [8-10]. As an extension of our program, we extended the spectroscopic study of the ethylene derivatives to polysubstituted halogenated ethylenes. In this paper we describe new results on the photoelectron spectroscopy (TPES and CIS) of the 1,1-$C_2H_2F_2$ molecular system using synchrotron radiation. The fixed-wavelength HeI-PES has been remeasured and reexamined in detail. The proposed interpretation and assignments are based on *ab initio* quantum chemical calculations.

2. Experimental details

2.1. Experimental setup

The experimental setup used in this work has already been described in detail elsewhere [10]. Only the most important features of the three experimental techniques used in the present experiments will be recalled in this section.

Except for the HeI-PES measurements, in the two other experiments reported here, we used the vacuum UV light from the synchrotron radiation provided by the electron storage ring BESSY (Berlin, Germany). This light is dispersed by a vacuum UV 3 m normal incidence (3 m NIM beam line) monochromator [11] equipped with a 2400 l mm^{-1} Pt grating. The entrance and exit slit widths were set from 50 to 200 μm depending on the signal intensity.

The light beam is focused into an ion chamber, in the focusing plane of a tandem electron spectrometer consisting of two 180° electrostatic deflectors. This electron energy analyser works at constant energy resolution, i.e. at constant pass energy E_0. The resolution at full width half-maximum is given by $AE/E_0 = w/104$ where w is the slit width expressed in millimeters. In the present experiments w = 0.5 or 1.0 mm and E_0 is set from 1.1 to 10.0 V depending upon the type of experiment and the signal intensity.

In addition to the synchrotron storage ring beam current, the photoelectron signal of a gold diode, inserted in the ion chamber opposite to the 3 m NIM monochromator exit slit, is recorded in order to normalize the photoelectron signals in the TPES and CIS spectra.

The first and most obvious operating mode of this experimental setup is the measurement of 'fixed-wavelength' photoelectron spectra. The HeI resonance line at 58.4 nm is produced in a microwave discharge and guided into the ionization region through a quartz capillary. Optimal conditions for resolution and intensity are obtained for a pass energy E_0 = 1.1 V providing a nominal resolution of 9 meV as measured on the $Xe^+(^2P_{3/2})$ peak.

The second operating mode is the measurement of 'constant photoelectron energy' spectroscopy. These are recorded by tuning the photon energy hv and keeping constant the energy $E^e_{kin}$of the electrons transmitted through the tandem electron energy analyser system. In the particular case of 'zero-kinetic energy' or 'threshold' (TPE) photoelectrons, the electron accelerating voltage V_{acc} is kept equal to E_0 as close as possible. This equality is optimized to obtain the highest TPE signal intensity. The TPE of the sample gas has been normalized to the photon transmission function of the monochromator by measuring simultaneously the photoelectron current intensity of the gold diode.

The third kind of experiment performed with this instrument is the CIS spectroscopy of vibrational and/or electronic states of molecular ions. The aim of this experiment is to measure the relative partial ionization cross-sections as a function of the photon energy for well-defined vibronic states of the molecular ion. It is well known that autoionization strongly perturbs photoionization and dissociative photoionization cross-sections by inducing dramatic variations in the distributions in the final ionic states. The running of a CIS spectrum requires to keep IE = hv-E^e_{kin} constant, i.e. the IE corresponding to the considered ionic state. The photon energy hv and the photoelectron kinetic energy E^e_{kin} must then be scanned in parallel. The details of the experimental procedure have been described earlier [10].

The commercially available 1,1-$C_2H_2F_2$, purchased from Fluochem Ltd and of 99.5% purity, was used

without further purification.

2.2. Data handling and error estimation

To improve the experimental resolution of the HeI-PES, the deconvolution technique has been applied to the original spectrum. A repeated iterative procedure [12] has been used allowing us to improve the effective resolution to about 10 meV as measured on the PES of 1,1-$C_2H_2F_2$.

As will be mentioned in the next sections, weak structures and diffuse peaks are often superimposed on a strong continuum. To make the characterization of these features easier, a 'continuum subtraction' procedure has been applied. This method has already been used successfully in previous spectral analyses [13]. For this purpose, the experimental curve is severely smoothed to simulate the underlying continuum which is then subtracted from the original photoelectron spectrum. The smoothing procedure consists in filtering the experimental curve by fast Fourier transform. The weak features then emerge from a strongly attenuated remaining background. The resulting diagram will be called Δ plot in the forthcoming sections.

In HeI-PES the photoelectron energy scale has been calibrated by recording the PES of a rare gases X/1,1-$C_2H_2F_2$ mixture (X = Ar, Kr and Xe). The rare gas IEs ($^2P_{3/2}$ and $^2P_{1/2}$ states) are used to calibrate the energy scale through a linear regression giving ± 1 meV precision on the energy. The first band has been recorded at different settings of E_0, i.e. at different resolutions of the tandem analyser. Under high-resolution conditions, the spectrum has been scanned by 3 meV increments.

The photon energy scale of the 3 m NIM monochromator has been calibrated with rare gas photoabsorption spectrum and/or TPES. An accuracy of better than 2-3 meV is achieved. For this purpose, Ar and/or Xe were used. To obtain the relative partial photoionization cross-sections, the CIS spectra have to be normalized to the transmission function of the monochromator and of the electron energy analyser. The former is recorded simultaneously with the CIS spectrum. The latter is obtained by recording the CIS curve of a rare gas, e.g. Xe^+ ($^2P_{3/2}$) exhibiting no structure over the same photon energy range as for the investigated molecular ion.

The error on the energy position of a feature is estimated to be 6 meV when the spectrum is recorded with energy increments of 5 meV, i.e. in the TPES and HeI-PES over large energy ranges. For the broad bands observed in these spectra, the position of the maxima (vertical IEs) is estimated with an accuracy of 10 meV. In the photoelectron spectra recorded with 3 meV increments over narrow energy ranges, the accuracy is estimated to be of about 5 meV including the energy scale precision. For the CIS spectra recorded with 10 meV increments, the position of the features is measured with an error estimated at 15 meV.

Figure 1. *(a) TPES of 1,1-$C_2H_2F_2$ between 10 and 28 eV photon energy. (b) HeI-PES of 1,1-$C_2H_2F_2$ at medium resolution. Vertical bars locate the vertical IEs.*

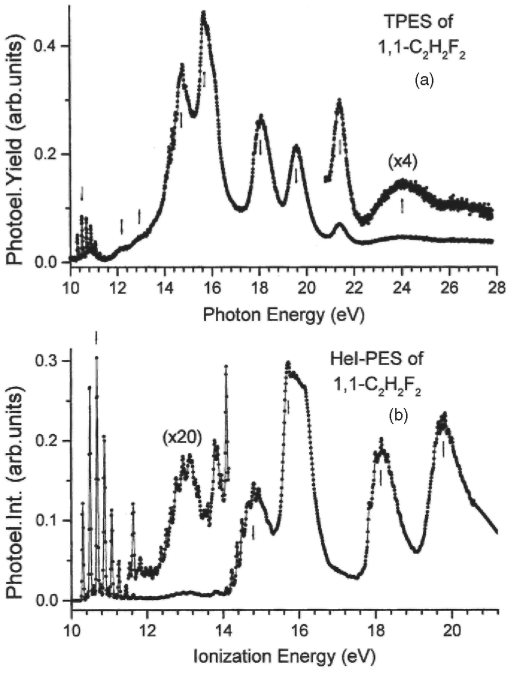

3. Experimental results

For ease in the discussion HeI, TPES and CIS spectra will be discussed separately.

3.1. The HeI and TPES

Figure 1 (a) shows the TPE spectrum of 1,1-$C_2H_2F_2$ as recorded over a wide photon energy range, i.e. from 8 to 28 eV, and with 5 meV energy increments. The upper limit was restricted by the grating transmission function.

Seven well-defined bands are observed at vertical IEs of 10.493 ± 0.006, 14.771 ± 0.006, 15.680 ± 0.006, 18.100 ± 0.006, 19.576 ± 0.006, 21.398 ± 0.006 and at about 24.05 ± 0.01 eV. Fairly strong features appearing as shoulders in the very strong band at 14.771 eV are measured at about 12.10 and 12.88 eV.

For comparison, the HeI-PES of 1,1-$C_2H_2F_2$ has been recorded over the whole IE region available with the HeI resonance line and at medium resolution, i.e. with a pass energy E_0 = 2.0 eV. The typical result is shown in figure 1(b), where the energy increment is 10 meV In this spectrum the vertical IEs are measured at 10.495 ± 0.01, 14.810 ± 0.01, 15.716 ± 0.01, 18.157 ± 0.01 and 19.820 ± 0.01 eV. A very unusual observation is that the HeI-PES shows a very weak but structured background between the first and second PES bands with two maxima near 13.01 and 13.78 eV successively. The former band exhibits a long sequence of structures.

In table 1 we compare for the HeI-, HeII-PES [1-3] and PIMS [6, 7] results reported in earlier papers with the HeI and the TPES results obtained in this work.

Dramatic differences between the HeI-PES and the TPES have to be highlighted. Compared to the intensity of the $\tilde{X}^2B_1$ band of the ionic ground state at 10.495 eV, the relative intensity of the PES bands related to the excited ionic states is considerably enhanced by resonant photoionization in the TPES. As already observed in the case of C_2H_3F [8], the intensity in the HeI-PES is shared between the ground and excited states of the ion, whereas the TPES is overwhelmingly dominated by the excited states between 12 and 20 eV.

Table 1. *Comparison between the vertical (adiabatic) IEs (eV) of 1,1-$C_2H_2F_2$ as obtained by HeI (54.8 nm or 21.22 eV), HeII (30.4 nm or 40.8 eV) and threshold photoelectron spectroscopy.*

Ionized	HeI/HeII-PES and PIMS[a]			This work[b]	
orbital [2,3]	[1]	[2,3]	[6,7]	HeI-PES	TPES
$\tilde{X}$, $2b_1^{-1}$	(10.31)		(10.29 ± 0.01)	(10.298)	(10.304)
	10.72	10.7		10.688[c]	10.493[c]
$\tilde{A}$, $5b_2^{-1}$	(14.06)			(14.085)	
	14.79	14.9		14.810	14.771
$\tilde{B}$, $8a_1^{-1}$	15.73	15.8		15.716	15.680
$\tilde{C}$, $4b_2^{-1}$		16.1			
$\tilde{D}$, $1a_2^{-1}$		16.1			
$\tilde{E}$, $7a_1^{-1}$	18.22	18.2		18.157	18.100
$\tilde{F}$, $1b_1^{-1}$		18.2			
$\tilde{G}$, $3b_2^{-1}$	19.68	19.7		19.820	19.576
$\tilde{H}$, $6a_1^{-1}$		21.5			21.398
$\tilde{I}$, $5a_1^{-1}$		25.2			24.05

[a] The uncertainty on the measurements are mentioned when specified by the authors.
[b] The uncertainty is evaluated to be ± 0.005 eV for HeI-PES and ±0.007 eV for TPES.
[c] For explanation, see the text in section 5.1.1.

3.2. The CIS photoelectron spectra

The CIS spectra corresponding to the successive electronic states of the molecular ion were recorded up to 10 eV above the corresponding vertical IEs, scanning by this way a 10-26 eV photon energy. Figure 2(a) displays the CIS spectra measured for the eight vibronic states of 1,1-$C_2H_2F_2^+$ as well as the TPES reference spectrum. For most electronic excited states, the CIS spectrum shows almost the same shape: it peaks at

threshold and shows a slow monotonic decrease for increasing photon energy. For the ease of interpretation and discussion, the photo-absorption spectrum (PAS) of 1,1-$C_2H_2F_2$ measured in the same energy range [14] is reproduced in figure 2(b).

A sequence of vibrationally resolved CIS spectra is shown in figure 3 for the most intense v_2 vibrational normal mode in the $\tilde{X}^2B_1$ ground ionic state. The CIS (v = 0) spectrum shows marked differences with the spectra corresponding to v = 1-3. The CIS spectra related to these latter vibrational levels look quite similar. Each of these spectra shows maxima near 13.1, 14.1, 14.6, 16.1 eV and a shoulder at about 15.0 eV. Above 17 eV a first broadband with a maximum is observed at 18.0 eV and a second band starts at 19.1 eV and extends probably above 20 eV photon energy. These latter characteristics are also observed in the CIS spectrum for v = 0. The CIS spectrum corresponding to the vibrationally excited $\tilde{X}^2B_1$ state at 12.9 eV, i.e. 1.18 eVbelow the adiabatic IE of the $\tilde{A}^2B_2$ state is very different.

Figure 2. *(a) TPES of 1,1-$C_2H_2F_2$ and CIS spectra at IEs of 10.45, 12.90, 14.77, 15.6, 16.00, 18.23, 19.74 and 21.56 successively. (b) PAS of 1,1-$C_2H_2F_2$ measured in the same photon energy range [14]. Boxes (a-e) indicate energy ranges of excited valence and Rydberg states.*

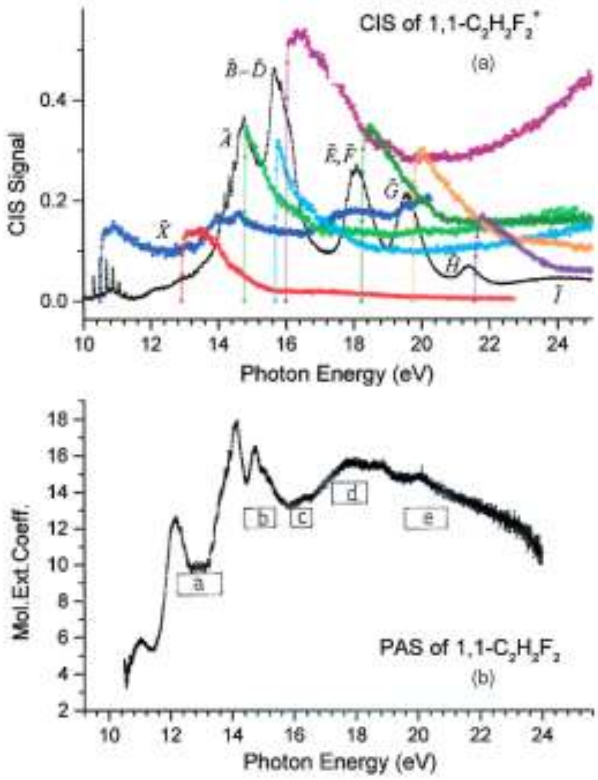

4. *Ab initio* calculations

4.1. Tools and methods

All calculations described in this work were performed with the GAUSSIAN (G03) program [16]. The electronic configuration of 1,1-$C_2H_2F_2$ in the C_{2v} point group is given by

$$F\left(1b_2^2 1a_1^2\right) - C\left(2a_1^2 3a_1^2\right)$$
$$(4a_1)^2(2b_2)^2(5a_1)^2(6a_1)^2(3b_2)^2(1b_1)^2(7a_1)^2(1a_2)^2$$
$$\times(4b_2)^2(8a_1)^2(5b_2)^2(2b_1)^2\tilde{X}^1A_1,$$

where $4a_1$ and $2b_2$ are the inner-shell valence orbitals on F and the rest are the outer-valence orbitals. The 6-31G**(5d) basis set was chosen for the calculations.

Figure 3. *Vibrationally resolved CIS spectra of 1,1-$C_2H_2F_2^+$($\tilde{X}^2B_1$) measured for the υ_2 vibrational mode (υ = 0-3) and at 12.9 eV.*

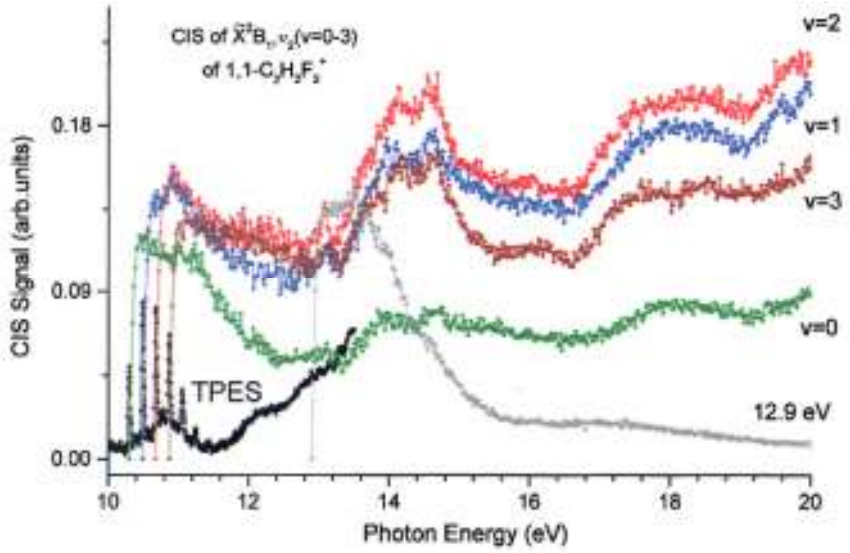

Figure 4. *Graphical representation and description of the 12 vibrational normal modes coordinates of 1,1-$C_2H_2F_2^+$ in the C_{2v} symmetry for which the associated wavenumbers have been calculated.*

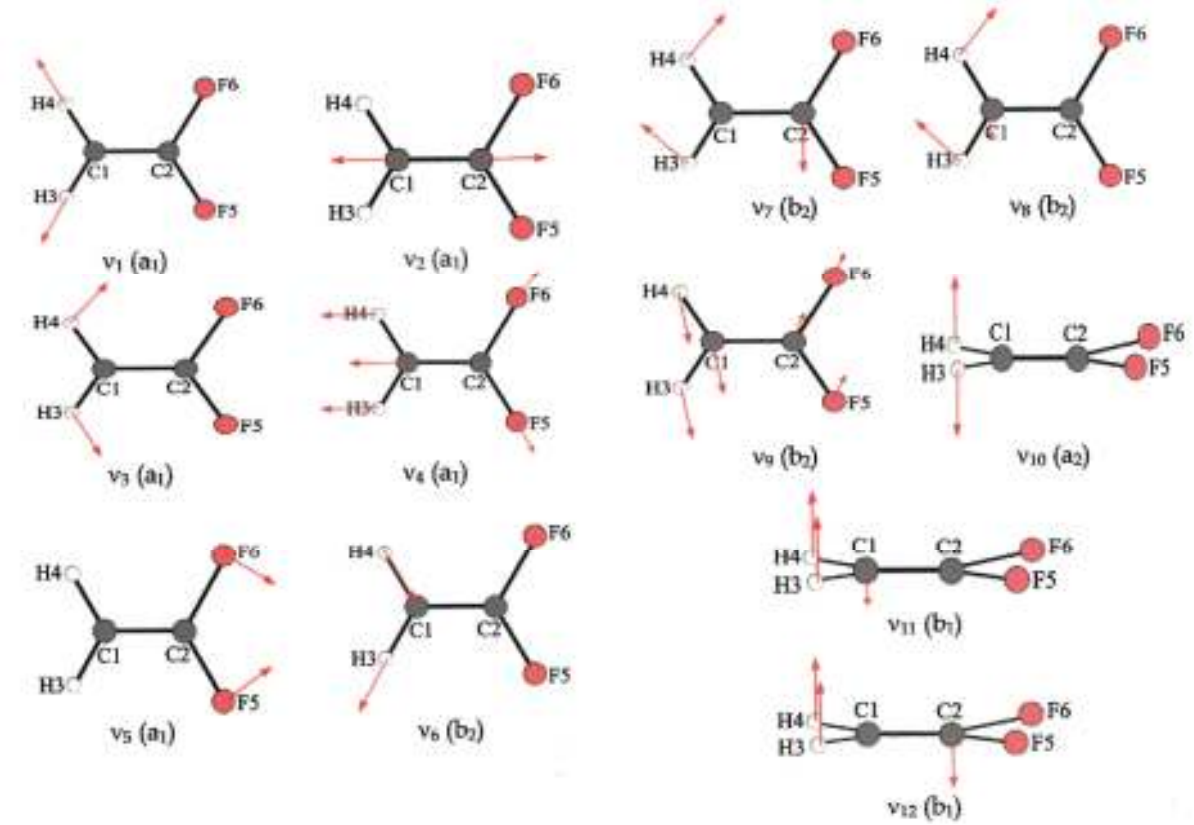

Two calculation levels were considered taking into account the dynamic electronic correlation (QCISD [17], B3LYP [18, 19]) or only the static electronic correlation (CASSCF [20-22]). The wavefunction related method QCISD was considered within the frozen core approximation, i.e. evaluating the electronic correlation with the valence electrons only. The CASSCF active space was defined as 10(9) electrons and 8 active MO for

the neutral (cation).

The geometry optimization was performed with the three calculation levels starting from the optimized geometry of the neutral. This was achieved for the lowest energy states of each symmetry representation of the C_{2v} point group, with the constraint of staying in the symmetry point group.

The vibrational wavenumbers characterizing the 12 vibrational normal modes of the neutral molecule and the molecular ion, as represented in figure 4, were determined at the B3LYP level.

4.2. Results of the calculations

The geometries optimized within the C_{2v} symmetry point group are presented in table 2. The CAS calculations on the $\tilde{C}$ state were only possible with the state average option because of its strong coupling with the two lower states.

The vibrational wavenumbers calculated at the B3LYP level for the 12 vibrational normal modes of the neutral and ionic ground states (see figure 4) are listed in table 3. For the $\tilde{X}^1A_1$ neutral ground state, the present results are compared to those obtained by Jiang *et al* [15] and in our earlier work [23], respectively. Table 4 displays the results related to the same molecular parameters for the first three ionic excited states.

Apart from the ground and first excited states, the electronic states of the cation are found to be transition states in the C_{2v} symmetry point group. A geometry optimization in the C_s symmetry point group was performed only for the $\tilde{C}^2B_2$ state, at the CAS level, because the other states were found to collapse on the $\tilde{A}^2B_2$ state (see table 2).

The shape of the singly occupied MO was obtained at the optimized geometry of the neutral molecule for the first six ionic states. These orbitals were calculated at the CAS(9,8)/6-31G** level with the state averaging over six states. These are represented in figure 5.

Table 2. *Optimized geometries of the neutral ground state of 1,1-$C_2H_2F_2$ and the first four ionic states of 1,1-$C_2H_2F_2^+$ calculated at three levels: inter-nuclear distances R in Å and angles in degrees. For the atomic numbering refer to the inset.*

Level	State	C1-C2	C1-H	C2-F	H-C1-C2	C1-C2-F
			Neutral ground state			
CAS(10,8)	$\tilde{X}^1A_1$	1.3210	1.0912	1.3069	119.477	124.952
QCISD		1.3253	1.0768	1.3322	119.728	125.015
B3LYP		1.3225	1.0805	1.3260	119.883	125.033
			Ionic states			
CAS(9,8)	$\tilde{X}^2B_1$	1.4107	1.0954	1.2393	118.539	122.366
QCISD		1.4176	1.0819	1.2706	118.755	122.292
B3LYP		1.4151	1.0869	1.2684	119.116	122.284
CAS(9,8)	$\tilde{A}^2B_2$	1.3450	1.1689	1.2667	139.935	121.950
QCISD		1.3288	1.1549	1.2935	141.190	121.982
B3LYP		1.3244	1.1617	1.2891	139.656	122.070
CAS(9,8)	$\tilde{B}^2A_1$ (a)	1.4292	1.1178	1.2610	103.944	119.611
QCISD		1.4035	1.0970	1.3042	107.916	119.795
B3LYP		1.3834	1.0995	1.3023	110.607	120.272
CAS(9,8)	$\tilde{C}^2B_2$ (b), (c)	1.3301	1.1072	1.3499	126.714	128.675
	$\tilde{C}^2A'$ (b), (c)	1.3266	1.1386	1.2685	127.588	131.960
			1.1190	1.4737	133.214	123.603
QCISD	(b)	VC	VC	VC	VC	VC
B3LYP	(b)	VC	VC	VC	VC	VC
CAS(9,8)	$\tilde{D}^2A_2$ (d)	1.3141	1.0942	1.3518	119.086	130.746
QCISD		1.3059	1.0819	1.4067	119.530	130.417
B3LYP		1.3014	1.0868	1.4017	119.882	129.754

(a). The $\tilde{B}$ ionic state in the C_{2v} point group symmetry is calculated as a transition state. A geometry optimization of this state in the C_S symmetry point group leads to the $\tilde{A}^2B_2$ state.
(b). The $\tilde{C}$ ionic state in the C_{2v} point group symmetry is calculated as a transition state. The minimum belongs to the C_S symmetry point group and cannot be determined at the B3LYP or QCISD level owing to variational collapse (VC).
(c). The $\tilde{C}$ ionic state could not be determined at the CAS level without a state average weighting. The weights used in the present calculations were 0.5 on the two $^2B_2$ states and 0.0 for the other states.
(d). The $\tilde{D}$ ionic state corresponds to a transition state in the C_{2v} point group symmetry.

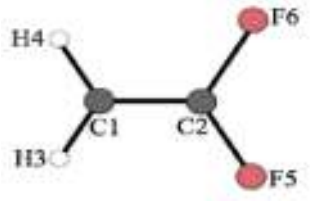

Figure 5. *Representation of the singly occupied MO as obtained at the CAS(9,8)/6-31G** level with state average on six states and at the optimized geometry of the neutral molecule for the (a)$\tilde{X}^2B_1$, (b)$\tilde{A}^2B_2$, (c)$\tilde{B}^2A_1$, (d)$\tilde{C}^2B_2$, (e)$\tilde{D}^2A_2$, (f)$\tilde{E}^2A_1$, (g)$\tilde{F}^2B_1$ and (h)$\tilde{G}^2B_2$ states. Contours correspond to 0.07 au density.*

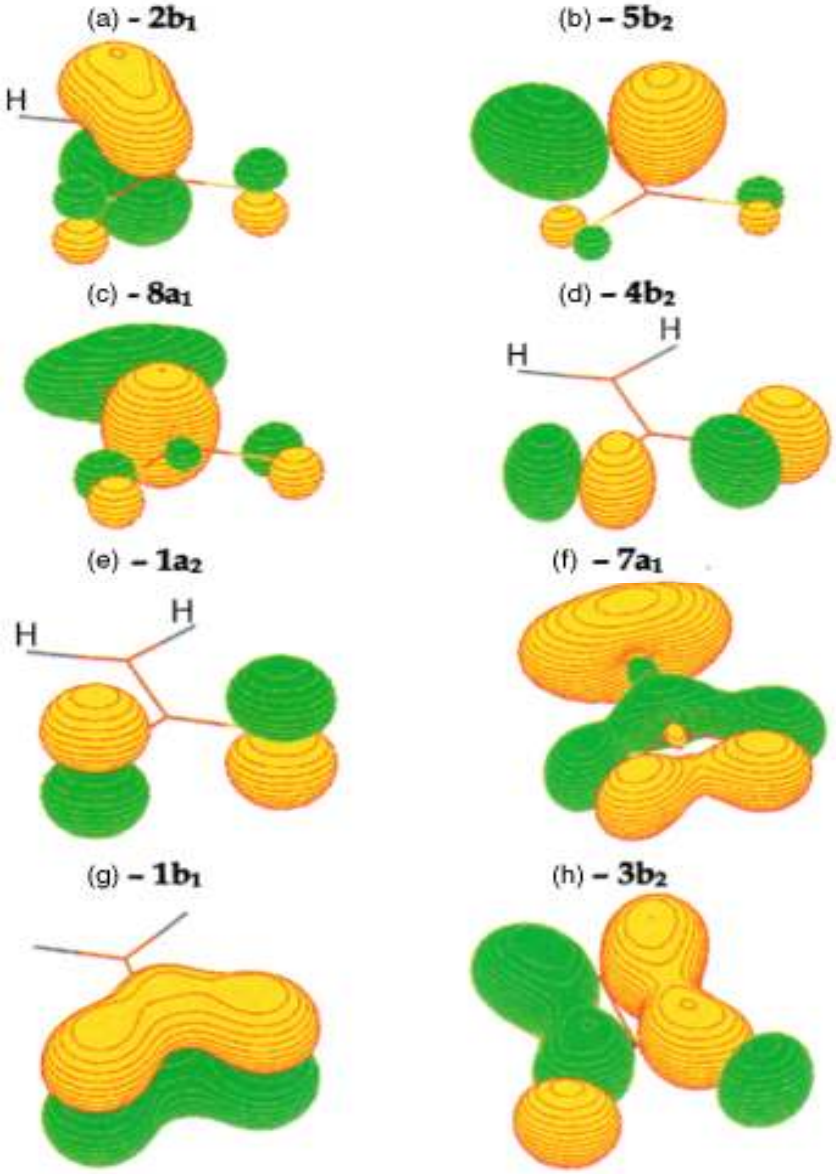

Published in : Journal of Physics : B Atomic Molecular & Optical Physics (2012), vol. 45, 115101.
Status : Postprint (Author's version)

5. Discussion of the experimental data

5.1. The HeI-PES

The HeI-PES represented in figure 1(b) is in very good agreement with that measured by Lake and Thompson [1]. The intensity is shared evenly between the ground and excited ionic states between 10.3 and 21.2 eV. All five resolved vibronic bands exhibit a more or less complex vibrational structure. Only the first band is clearly dominated by one progression of eight well-resolved vibrational structures separated by weak to very weak peaks as shown in figure 6.

The position in energy of these structures, as averaged over five measurements carried out in different operating conditions, is listed in table 5 together with the associated standard deviations.

Figure 6. *The first photoelectronic band of 1,1-$C_2H_2F_2$ as observed between 10.2 and 11.8 eV and its vibrational analysis (vertical bars).*

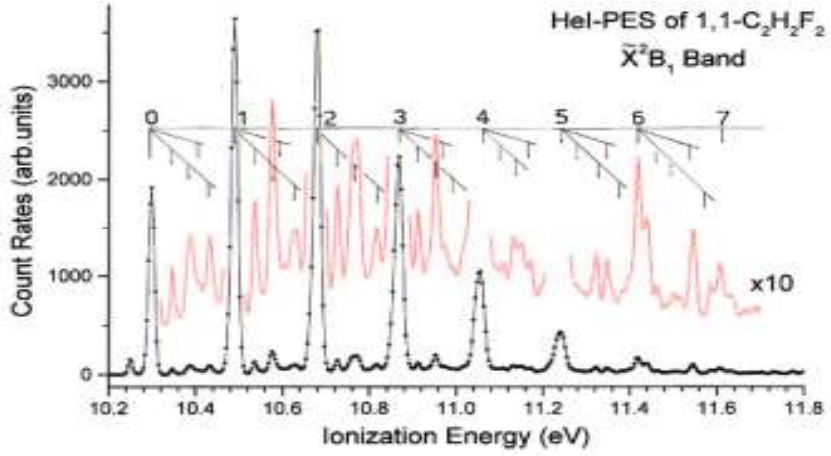

Figure 7. *Δ plots (a)-(e) of the HeI-PES bands related to the 1,1-$C_2H_2F_2^+$ electronic excited states between 11.8 and 20.7 eV. The vibrational analyses are indicated by vertical bars.*

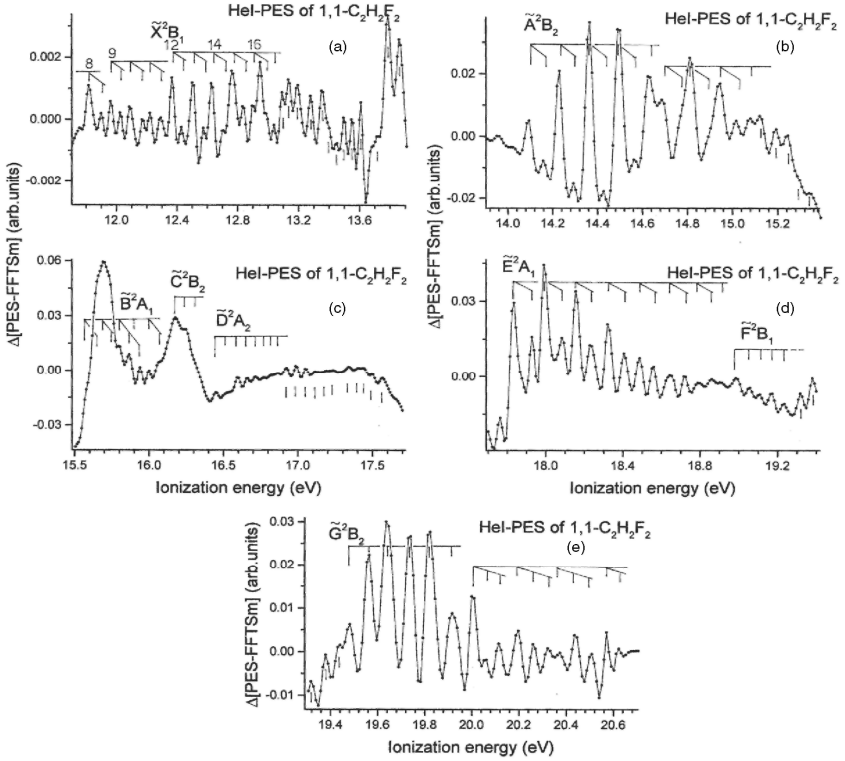

Table 3. *Ab initio (B3LYP/6-31G** (5d)) calculated wavenumbers (cm^{-1}) associated with the 12 vibrational normal modes (VibrNM) (represented in figure 4 for the 1,1-$C_2H_2F_2^+$ ($\tilde{X}^2B_1$) state) related to the neutral ground state of 1,1-$C_2H_2F_2$ and the ionic ground state of 1,1-$C_2H_2F_2^+$, respectively. The atomic numbering in 1,1-$C_2H_2F_2$ refers to the figure in table 2. Comparison is made with previous calculations [15, 23] and present determinations.*

1,1-$C_2H_2F_2$-$\tilde{X}^1A_1$				
VibrNM	Wavenumber (cm^{-1})			VibrNM Description
	Exper.	Theory		
	[15]	[15]	This work	
a_1 symm.				(see figure 4)
ν_1	3053	3092	3220	C-H symm. stretch
ν_2	1730	1747	1798	C = C and C-F stretching H-C-H and F-C-F bending
ν_3	1354	1379	1421	H-C-H bending
ν_4	916	923	948	C-F symm. stretching
ν_5	544	562	543	F-C-F bending
b_2 symm.				
ν_6	3170	3185	3321	C-H antisymm. stretching
ν_7	1303	1331	1351	C-F antisymm. stretching H-CC antisymm. bending
ν_8	949	946	965	H-CC antisymm. bending
ν_9	430	443	436	F-CC antisymm. bending
a_2 symm.				
ν_{10}	714	704	723	H out-of-plane twisting
b_1 symm.				
ν_{11}	806	791	818	H out-of-plane rocking
ν_{12}	601	621	630	C = C out-of-plane
1,1-$C_2H_2F_2$+-$\tilde{X}^2B_1$				
Vibr.NM	Wavenbr (cm^{-1})			VibrNM description
	Exp	Theory		
		This work	MP2 [23]	
a_1 symm.				(see figure 4)
ν_1	-	3169	3264	C-H symm. stretch
ν_2	1573 ± 8	1593	1653	C = C and C-F Stretching H-C-H and F-C-F bending
ν_3	-	1438	1479	H-C-H bending
ν_4	895 ± 16	965	981	C-F symm. stretching C = C stretching
ν_5	532 ± 56	573	582	F-C-F bending C-F symm. stretching
b_2 symm.				
ν_6	-	3299	3408	C-H antisymm. stretching
ν_7	-	1564	1602	C-F antisymm. stretching H-CC antisymm. bending
ν_8	-	1009	1039	H-CC antisymm. bending
ν_9	395 ± 32	413	419	F-CC antisymm. bending
a_2 symm.				
ν_{10}	-	375	382	H out-of-plane twisting
b_1 symm.				
ν_{11}	-	915	911	H out-of-plane rocking
ν_{12}	-	621	646	C = C out-of-plane

5.1.1. The first PES band: the $\tilde{X}^2B_1$ state (see figures 6 and 7(a)).

The first strong band is very unexpectedly followed by a long sequence of very weak structures filling the energy gap between the first and second PES bands. These features are expected to belong to the ground ionic state. This part of the PES is highlighted in figure 1(b) with an amplification factor of 20. The energy position of the observed features is listed in table 5 and is clearly located in the Δ plot in figure 7(a).

The strong low-energy part of the first PES band is assigned to the ionization of the highest occupied $2b_1$ orbital with a predominant C = C π orbital character giving rise to the $\tilde{X}^2B_1$ ground state of the 1,1-$C_2H_2F_2^+$ cation. The experimental adiabatic and vertical IEs are $IE_{ad}(1,1\text{-}C_2H_2F_2^+,\tilde{X}^2B_0)$ = (10.298 ± 0.001) eV and $IE_{vert}(1,1\text{-}C_2H_2F_2^+,\tilde{X}^2B_1)$ = (10.688 ± 0.001) eV, respectively. The energy separation ΔG_v between the strongest features in the first PES band have been plotted versus the vibrational quantum number *v*. The experimental data are best fitted by the relation (least-squares fit with $\chi^2 = 3.1 \times 10^{-6}$):

$$\mathrm{IE} = 10.299(\pm 0.0014) + 0.195(\pm 0.0010) \times v - 0.000\,96(\pm 0.000\,14) \times v^2. \quad (1)$$

Table 4. *Ab initio (B3LYP/6-31G** (5d)) in this work and MP2 [23] calculated wavenumbers (cm^{-1}) associated with the 12 vibrational motions (VibrNM) (represented in figure 4 for the 1,1-$C_2H_2F_2^+$($\tilde{X}^2B_1$ state)) related to the $\tilde{A}^2B_2$, $\tilde{B}^2A_1$ and $\tilde{D}^2A_2$ states successively. For the atomic numbering in 1,1-$C_2H_2F_2$ refer to the figure in table 2.*

VibrNM	B3LYP Wavenbr. (cm^{-1})	MP2 [23] Wavenbr. (cm^{-1})	Exp. this work Wavenbr. (cm^{-1})	VibrNM description
		1,1-$C_2H_2F_2^+$-$\tilde{A}^2B_2$		
a_1 symm.				
ν_1	2749	2849	-	C-H symm.stretching
ν_2	1715	1793	-	C = C stretching
ν_3	1080	1173	1077 ± 56[a]	H-C-H and F-C-F bending H-C-H bending
ν_4	986	1051	-	H-C-H bending and C-F stretching
ν_5	531	546	532 ± 40	F-C-F bending
b_2 symm.				
ν_6	2242	2328	-	C-H antisymm stretching
ν_7	1368	1468	-	C-F antisymm stretching
ν_8	534	614	-	H-CC antisymm. bending
ν_9	279	322	-	F-CC antisymm. bending
a_2 symm.				
ν_{10}	946	893	-	H out-of-plane twist
b_1 symm.				
ν_{11}	657	698	661 ± 32	C2 out-of-plane
ν_{12}	328	336	-	H out-of-plane in phase
VibrNM	B3LYP Wavenbr. (cm^{-1})	MP2 [23] Wavenbr. (cm^{-1})	Exp. this work Wavenbr. (cm^{-1})	VibrNM description
		1,1-$C_2H_2F_2^+$-$\tilde{B}^2A_1$(TS)		
a_1 symm.				
ν_1	2958	3003	-	C-H symm. stretching
ν_2	1367	1529	-	C = C stretching
ν_3	1213	1158	-	H-C-H bend and F-C stretch H-C-H bending
ν_4	871	969	839 ± 32	C = C stretching and C-F stretching
ν_5	517	513	540 ± 32	C = C stretch, F-C-F bending and C-F stretching
b_2 symm.				
ν_6	2839	3197	-	C-H antisymm stretching
ν_7	1168	1262	-	C-F antisymm stretching
ν_8	534	606	-	H-CC bending F-CC antisymm. bending
ν_9	**i 1459**	**i 1267**	-	**H-CC antisymm. bending**
a_2 symm.				
ν_{10}	633	597	-	H out-of-plane twist
b_1 symm.				
ν_{11}	751	685	-	In phase H out-of-plane

ν_{12}	502	223	-	Complex out-of-plane motion
	B3LYP	MP2 [23]	Exp. this work	
VibrNM	Wavenbr. (cm^{-1})	Wavenbr. (cm^{-1})	Wavenbr. (cm^{-1})	VibrNM description
			1,1-$C_2H_2F_2^+$-$\tilde{D}^2A_2$(TS)	
a_1 symm.				
ν_1	3175	3258		C-H symm. stretching
ν_2	1795	2088		C = C and C-F stretching
				F-C-F Bending
ν_3	1386	1415		H-C-H bending
ν_4	840	826		C-F stretching
			(621 ± 24)[b]	
ν_5	460	448		F-C-F bending
b_2 symm.				
ν_6	3277	3366		C-H antisymm. stretching
ν_7	936	955		H-CC antisymm. bending
ν_8	408	412		F-CC antisymm. bending
ν_9	**i 494**	**i 430**		**F-C antisymm. stretching**
a_2 symm.				
ν_{10}	721	844		H out-of-plane twist
b_1 symm.	959	1138		In phase H out-of-plane
ν_{11}	540	643	(621 ± 24)[b]	Complex out-of-plane motion

[a] Averaged value between 1089 and 1065 cm^{-1}.
[b] For explanation of this assignment, see the text.

This fit provides us with a (0,0) transition energy of 10.299 ± 0.001 eV, close to the experimental adiabatic IE_{ad} = 10.298 ± 0.001 eV listed in table 1. The value of 1573 ± 8 cm^{-1} (0.195 ± 0.001 eV) has to be compared with 1593 cm^{-1} = $\omega_2(a_1)$ (C = C stretching, H_2C and F_2C bending: see figure 4) vibration predicted by the present *ab initio* calculations (see table 3) at the B3LYP/6-31G**(5d) level in the C_{2v} point group. In an earlier theoretical work at the MP2 level, the wavenumber of 1653 cm^{-1} was obtained [23]. Finally this relation provides us also with the anharmonicity constant $\omega_2 x_2$ = 7.7 ± 1.1 cm^{-1} (or 0.000 96 ± 0.000 14 eV).

The value of 10.299 eV has to be compared with the IE_{ad} reported by Lake and Thompson [1] at 10.31 eV, without any uncertainty indication, and Reinke *et al* [6] at 10.29 ± 0.01 eV. The experimental vertical IE value is of 10.688 ± 0.001 eV (see figure 1) or 10.494 ± 0.001 eV (see figure 6) corresponding to $2\upsilon_2$ and υ_2, respectively. The main difference between the two recordings is the dwell time of 10 and 50 s: a pressure drift in the latter experiment could be the reason for the small difference in intensities. These IE values have to be compared with 10.72 eV [1] and 10.7 eV [2, 3] reported earlier.

The fundamental wavenumber of 1573 ± 8 cm^{-1} determined in this work has to be compared with the only value of 1600 cm^{-1} reported by Lake and Thompson [1]. The agreement is satisfactory. It has to be mentioned here that this wavenumber is nearly equal (within the uncertainty limits) to that determined for the $C_2H_3F^+$ cation for which the C = C stretching vibration is characterized by ω_4 = 1565 ± 16 cm^{-1} (0.194 ± 0.002 eV) [8]. From this comparison the force constant of the C = C bond is not appreciably, if not at all, strengthened by the geminal fluorine substitution.

As shown in table 5 and figure 6, the very weak features are tentatively assigned founding the arguments on the present *ab initio* calculations (see table 4). Besides $hc\omega_2$ (a_1) = 195 meV (1573 cm^{-1}), two energy intervals have to be mentioned: 395 ± 32 cm^{-1} (49 ± 4 meV) and 895 ± 16 cm^{-1} (111 ± 2 meV). Comparing with the calculated values, they can be assigned to $\omega_9(b_2)$ = 413 cm^{-1} and $\omega_4(a_1)$ = 965 cm^{-1} (C-F symmetric stretch and C = C stretch), respectively (see table 3), the latter mode being related to the nature of the orbital involved in the ionization, the $2b_1$ having a C = C bonding and a C-F antibonding character (see figure 5(a)).

None of these two wavenumbers could be compared with the value ω = 720 cm^{-1} reported by Lake and Thompson [1] and assigned to the C-F symmetric stretching mode. However, if this value could be considered as 2ω, i.e. 2 × 360 cm^{-1} the agreement becomes fairly good. On the other hand, no wavenumber at 720 cm^{-1} results from *ab initio* calculations: the C-F symmetric stretching wavenumber is calculated at 965 cm^{-1} when combined with C = C stretching or at 573 cm^{-1} when combined with F-C-F bending (see figure 4 and table 3).

As mentioned earlier in this section, a significant photoelectron signal is detected between 10.6 and 14.0 eV. The subtraction method (see section 2.2) leads to the Δ plot in figure 7(a). The energy positions of all the features are listed in table 5.

Clearly, this part of the HeI-PES has to be assigned to the ground state of the cation. The first excited ionic state has been calculated earlier [23] from 3.6 to 5.0 eV above the ground state, depending upon the calculation level but in agreement with previous reports [2, 3].

An explanation for this very weak but extended vibrational structure of the ground ionic state is its sequential population through an intermediate neutral (e.g. Rydberg) state resonant with the HeI resonance line at 58.43 nm (21.22 eV). This phenomenon has been highlighted in diatomic and triatomic [12, 24] molecules using other rare gas resonance lines, e.g. the NeI lines at 73.58-74-37 nm (16.85-16.87 eV). The major result is usually a considerable extension of the vibrational structure whose intensity distribution depends mainly on the Franck-Condon overlap between the intermediate neutral and the final ionic states. For the assignment, one has to consider at least that the upper part of the potential hyper surface of the ground state is involved and the Franck-Condon region from the neutral excited intermediate state is very likely different from that starting from the neutral ground state.

If the v_2 progression in the first PES band extends up to 11.816 and 11.899 eV, corresponding to $8v_2$ and $8v_2 + 2v_9$, respectively, the contribution of autoionization could start at 11.961 eV which is designated as IE in table 5. Furthermore, between 11.961 and 12.293 eV, a very weak intensity variation could be observed. Energy intervals of about 0.135 ± 0.009 and 0.072 ± 0.010 eV or 0.066 ± 0.005 eV peak-to-peak intervals are measured. From 12.365 (designated as IE_1 in table 5) to 13.039 eV, an intensity alternation becomes obvious. For the major peak structure, an interval of 0.133 ± 0.007 eV is determined. The weaker structure is measured at 0.070 ± 0.006 eV. Both values are identical within error limits to those measured between 11.961 and 12.293 eV.

Table 5. *Energy (eV) in the HeI-PES and TPES and assignments for the structures observed in the first band corresponding to the 1,1-$C_2H_2F_2^+$($\tilde{X}^2B_1$) state: (0,0) means the vibrationless level.*

HeI-PES	TPES[a]	Assignments
10.298 ± 0.001	10.303	**0-0**
10.347 ± 0.004	-	v_9
10.389 ± 0.004	10.372	$2v_9$
10.409 ± 0.005	10.407	v_4
10.432 ± 0.003	-	$3v_9$
10.494 ± 0.001	10.490	$\boldsymbol{v_2}$
10.539 ± 0.003	-	$v_2 + v_9$
10.576 ± 0.004	10.570	$v_2 + 2v_9$
10.603 ± 0.003	10.595	$v_2 + v_4$
10.620 ± 0.008	10.620	$v_2 + 3v_9$
10.688 ± 0.001	10.682	$\boldsymbol{2v_2}$
10.728 ± 0.004	-	$2v_2 + v_9$
10.771 ± 0.004	10.778	$2v_2 + 2v_9$
10.818 ± 0.008	-	$2v_2 + 3v_9$
10.877 ± 0.002	10.871	$\boldsymbol{3v_2}$
10.916 ± 0.004	-	$3v_2 + v_9$
10.958 ± 0.003	10.951	$3v_2+2v_9$
10.974 ± 0.005	-	$3v_2$ + ?
10.989 ± 0.005	10.986	$3v_2 + v_4$
10.016 ± 0.006	-	$3v_2 + 3v_9$
11.064 ± 0.002	11.060	$\boldsymbol{4v_2}$
11.111 ± 0.003	-	$4v_2 + v_9$
11.150 ± 0.003	11.164	$4v_2 + 2v_9$
11.177 ± 0.008	-	$4v_2 + v_4$
11.249 ± 0.002	11.254	$\boldsymbol{5v_2}$
11.321 ± 0.005	-	$5v_2 + 2v_9$
11.348 ± 0.005	-	$5v_2+ v_4$
11.399 ± 0.006	-	$5v_2 + 3v_9$
11.418 ± 0.001	-	na

11.438 ± 0.005	11.436	**$6\nu_2$**
11.461 ± 0.005	-	$6\nu_2$ + ?
11.500 ± 0.005	-	$6\nu_2$ + ?
11.547 ± 0.005	-	$6\nu_2 + \nu_4$
11.586 ± 0.005	-	$6\nu_2 + 3\nu_9$
11.620 ± 0.005	11.621	**$7\nu_2$**
HeI-PES[a]	TPES[b]	Assignments
11.620	11.609	**$7\nu_2$**
11.754	-	$7\nu_2 + \nu_4$
11.816	11.821	**$8\nu_2$**
11.899	-	$8\nu_2 + 2\nu_9$
11.961	-	**IE($9\nu_2$)[c]**
12.023	-	$9\nu_2 + \nu_5$
12.092	-	**$10\nu_2$**
12.174	-	$10\nu_2 + \nu_5$
12.220	-	**$11\nu_2$**
12.293	-	$11\nu_2 + \nu_5$
12.365	-	**$IE_1(12\nu_2)$[c]**
12.428	-	$IE_1 + \nu_5$
12.505	-	**$13\nu_2$**
12.573	-	$13\nu_2 + \nu_5$
12.630	-	**$14\nu_2$**
12.702	-	$14\nu_2 + \nu_5$
12.760	-	**$15\nu_2$**
12.837	12.804	$15\nu_2 + \nu_5$
12.899	12.893	**$16\nu_2$**
12.946	-	$16\nu_2 + \nu_5$
13.039	13.017	**$17\nu_2$**
13.091	-	na[d]
13.132	-	na[d]
13.189	13.155	na[d]
13.277	13.293	na[d]
13.355	-	na[d]
13.448	13.446	na[d]
13.495	-	na
13.546	13.560	na
13.609	13.619	na
13.723	-	na
13.785	13.752	na
13.857	13.885	na
13.955	13.942	na
14.023	14.022	na

[a] Uncertainty estimated at ± 0.005 eV.
[b] Uncertainty estimated at ± 0.007 eV.
[c] For the explanation, see section 5.1.1.
[d] For the explanation, see section 5.1.1.

To account for this continuity, it is reasonable to assign the vibrational normal mode ν_2 (see figure 4) to the strongest vibrational transition, but corrected for its anharmonicity. Taking into account, in an IE-versus-υ diagram, the 12.293 eV (IE = $9\nu_2$), 12.365 eV ($IE_1 = 12\nu_2$) and 13.039 eV ($17\nu_2$) transitions in addition to the $0\nu_2$ - $7\nu_2$ transitions previously considered (equation (1)), the best fit is given by (least-squares fit with $\chi^2 = 3 \times 10^{-3}$)

$$\begin{aligned} \mathrm{IE} = {} & 10.298(\pm 0.003) + 0.198(\pm 0.003) \\ & \times \upsilon - 0.0017(\pm 0.0002) \times \upsilon^2. \end{aligned} \qquad (2)$$

This relation is close to (1) obtained over the seven first vibrational quanta. The observed wavenumber of 564 cm^{-1} (0.070 eV) would still be assigned to the ν_5 normal mode.

5.1.2. The second PES band: the $\tilde{A}^2B_2$ state (see figure 7(b)).

The second HeI-PES band of 1,1-$C_2H_2F_2$ is shown in figure 1(b) and corresponds to the removal of one electron from the $5b_2$ orbital giving rise to the first excited $\tilde{A}^2B_2$ state of the ion (see figure 5(b)). The adiabatic IE is measured at 14.090 ± 0.005 eV, whereas the vertical value is at 14.810 ± 0.005 eV. These values have to be compared to IE_{ad} = 14.06 eV [1] and IE_{vert} = 14.79 eV [1] or 14.9 eV [2, 3]. By quantum chemical calculations, vertical IEs are predicted at 14.53-15.33 eV depending on the calculation level [2, 3].

Figure 7(b) shows the Δ plot related to the second HeI-PES band clearly displaying the vibrational structure up to 15.2 eV. The positions in energy of these features are listed in table 6.

The vibrational structure of the electronic state corresponding to this band displays two different regimes: (i) between 14.09 and 14.629 eV where structures are separated by 0.135 ± 0.007 eV (or 1089 ± 60 cm^{-1}) and 0.066 ± 0.005 eV (or 532 ± 40 cm^{-1}) with strong intensity alternations and a regular bell-shaped intensity distribution and (ii) between 14.686 eV (designated by IE in table 6) and 15.080 eV where intervals are of 0.132 ± 0.007 eV (or 1065 ± 60 cm^{-1}) and 0.082 ± 0.004 eV (or 661 ± 30 cm^{-1}) with regularly decreasing intensities. We suspect that the change of regime is linked to a vibronic perturbation discussed below. In both parts, and considering the uncertainty limits, very likely the same vibrational motion should be active at 1089 ± 60 or 1065 ± 60 cm^{-1}. The average value of 1077 cm^{-1} can be compared to the calculated value of 1080 cm^{-1} associated with the H-C-H bending mode (table 5). The two lower wavenumbers at 532 and 661 cm^{-1} should correspond to different modes considering the uncertainty limits. In their paper, Lake and Thompson [1] reported only one vibrational wavenumber of 1180 cm^{-1} without any error limit and assignment.

In an earlier paper about the dissociation dynamics of 1,1-$C_2H_2F_2^+$ [23], the potential energy surface of the $\tilde{A}^2B_2$ state has been investigated. It corresponds to the ionization of the $5b_2$ orbital (C-H bonding, H-H antibonding: see figure 5(b)). It is predicted to be very stable with a deep well but with a very small H-C-H angle of about 78°. This result is consistent with the PES: the H-C-H bending vibration is predicted with 1080 or 1173 cm^{-1} (see table 4). The perturbation observed in the vibrational progression in this PES band could be related to non-adiabatic interactions leading to internal energy conversion and possibly to fast predissociation. Three conical intersections were found involving the $\tilde{A}^2B_2$ state interacting with $\tilde{X}^2B_1$, $\tilde{B}^2A_1$ and $\tilde{C}^2B_2$ states [23].

Table 6. *Energy (eV) in the HeI-PES and TPES and assignments for the structures observed in the second band corresponding to the 1,1-$C_2H_2F_2^+$ ($\tilde{A}^2B_2$) state: (0,0) means the vibrationless level.*

HeI-PES[a]	TPES[b]	Assignments
14.090	14.071	0-0
14.158	14.151	ν_8
14.230	14.201	ν_3
14.292	14.280	$\nu_3+\nu_5$
14.365	14.330	$\mathbf{2\nu_3}$
14.427	14.400	$2\nu_3+\nu_5$
14.490	14.479	$\mathbf{3\nu_3}$
14.562	14.528	$3\nu_3+\nu_5$
14.629	14.608	$\mathbf{4\nu_3}$
14.686	14.657	IE
14.770	14.767	IE+ν_{11}
14.810	-	IE+ν_3
14.893	14.876	(IE+ν_3)+ν_{11}
14.940	14.915	IE+$\mathbf{2\nu_3}$
15.018	15.000	(IE+$2\nu_3$)+ν_{11}
15.080	15.074	IE+$\mathbf{3\nu_3}$
15.121	15.104	na
15.194	-	na
15.240	15.223	na
15.287	-	na
15.339	15.303	na

[a] Uncertainty estimated at ± 0.005 eV.
[b] Uncertainty estimated at ± 0.010 eV.

Table 7. *Energy (eV) in the HeI-PES and TPES and assignments for the structures observed in the third band corresponding to the 1,1-$C_2H_2F_2^+$($\tilde{B}^2A_1,\tilde{C}^2B_2,\tilde{D}^2A_2$) state: (0,0) means the vibrationless level.*

HeI-PES	TPES	Assignments
15.587	_	**$IE_1(\tilde{B}(0,0))$**[b]
15.660	-	$IE_1+\nu_8$
15.696	15.680	**$IE_1+\nu_4$**
15.727	15.759	$IE_1+\nu_4+\nu_8$
15.795	15.809	**$IE_1+2\nu_4$**
15.867	15.858	$IE_1+2\nu_4+\nu_8$
15.940	15.927	$IE_1+2\nu_4+2\nu_8$
16.002	16.007	**$IE_1+4\nu_4$**
16.064	16.057	$IE_1+4\nu_4+\nu_8$
16.178	16.166	**$IE_2(\tilde{C}(0,0))$**[b]
16.240	-	$IE_2+\nu_8$
16.302	-	$IE_2+2\nu_8$
16.447	-	**$IE_3(\tilde{D}(0,0))$**[b]
16.520	-	$IE_3+\nu_i$
16.597	-	$IE_3+2\nu_i$
16.659	-	$IE_3+3\nu_i$
16.717	-	$IE_3+4\nu_i$
16.768	-	$IE_3+5\nu_i$
16.820	-	$IE_3+6\nu_i$
16.867	-	$IE_3+7\nu_i$
16.924	-	**IE_4**[b]
16.986	-	na[a]
17.053	-	na[a]
17.121	-	na[a]
17.193	-	na[a]
17.235	-	na[a]
17.338	-	na[a]
17.405	-	na
17.441	-	na
17.494	-	na
17.566	-	na

[a] For the discussion, see section 5.1.3.
[b] For the explanation, see section 5.1.3.

The assignment of ω = 532 ± 40 cm^{-1} is less obvious. Two vibrational modes have to be considered, i.e. $\nu_5(a_1)$ and $\nu_8(b_2)$ (see table 4 and figure 4). Transitions involving the former are allowed whereas the latter is forbidden. This argument would strongly favour $\nu_5(a_1)$ though the weakness of the transitions would not totally exclude the involvement of $\nu_8(b_2)$.

The wavenumber of 661 ± 32 cm^{-1} should be assigned to $\nu_{11}(b_1)$ involving a C = C out-of-plane motion (see figure 4) based on the only possible comparison with the predicted value of 657 cm^{-1} (this work) or to 698 cm^{-1} [23] (see table 4). This possibility could occur only due to a non-adiabatic coupling as stated above.

5.1.3. The third PES band: the $\tilde{B}^2A_1,\tilde{C}^2B_2$ and $\tilde{D}^2A_2$ states (see figure 7(c)).

Extrapolating the low-energy side of the third PES band, an $IE_{ad} \approx 15.40$ eV could be estimated. From the Δ plot shown in figure 7(c), an IE_{ad} = 15.587 eV (designated by IE_1 in table 7) is obtained. The lowest vertical IE is equal to 15.696 ± 0.005 eV. A second maximum is observed at IE_{vert} = 16.178 ± 0.005 eV (IE_2 in table 7) and a very broad-and weak band would has a maximum around 17.0 eV. Above the onset at 15.78 eV, several shoulders and maxima are observed whose intensity is not regularly distributed.

To assign these energy values, the results of past quantum mechanical calculations are useful [2, 3, 23]. In the energy range of interest, the $\tilde{B}^2A_1$ ($8a^{-1}$) (IE_{vert} = 14.78-15.95 eV), $\tilde{C}^2B_2$ ($4b_2^{-1}$) (IE_{vert} = 15.74-16.17 eV) and $\tilde{D}^2A_2$ ($1a_2^{-1}$) (IE_{vert} = 15.28-16.57 eV) states have been identified. Furthermore, the vibrational wavenumbers corresponding to the $\tilde{B}^2A_1$ and the $\tilde{D}^2A_2$ have been calculated earlier [23]. Both results are summarized in table4. It should be pointed out that they must be considered as qualitative guides only because these two states are transition states in their C_{2v} geometry, i.e. showing both one imaginary wavenumber.

As shown in figure 7(c) and table 7 in the 15.6-16.1 eV IE range, two wavenumbers could clearly be identified, i.e. ω_1 = 839 ± 32 cm^{-1} (104 ± 4 meV) and ω_2 = 540 ± 32 cm^{-1} (67 ± 4 meV) and with the maximum intensity at 15.696 eV corresponding to the IE_{vert}. They can be related to the ν_4 and ν_5 calculated wavenumbers (table 4), also compatible with the shape of the 8ai ionized MO (see figure 5(c)). The opening of the $C_2HF_2^+$ dissociation channel [7] could explain the slightly resolved structures appearing as 'shoulders' in the 15.696 eV peak.

The only previous experimental determination in this energy range has been published by Lake and Thompson [1] who reported one wavenumber of 1290 cm^{-1}. This should be compared with the present 839 ± 32 and 540 ± 32 cm^{-1} wavenumbers whose sum, 1379 ± 32 cm^{-1}, is in fair agreement with the early reported value.

From 16.064 to 16.447 eV, a structured peak is observed in the Δ plot (see figure 7(c)). The maximum of this peak at 16.178 eV (IE_2 in table 7) also corresponds to the AE of the CH_2^+ fragment at 16.30 eV [6, 7]. This PES signal could be assigned to the $\tilde{C}^2B_2$ state of 1,1-$C_2H_2F_2^+$.

Quantum chemical calculations at the QCISD [23] or at the B3LYP level in the C_{2v} symmetry point group failed to calculate the geometry and the vibrational wavenumbers because the $\tilde{A}^2B_2$ and the $\tilde{C}^2B_2$ have the same symmetry. Shoulders are clearly identified in the PES peak at an interval of about 62 meV (500 cm^{-1}) (see figure 7(c)). As for the lower lying ionic states, several vibrational motions are characterized by a wavenumber of about 500 cm^{-1}. The $4b_2$ MO is F-F antibonding (see figure 5(d)) and the F-C-F symmetric or antisymmetric bending vibration is characterized by a wavenumber of the order of 500 cm^{-1}.

At 16.447 eV (IE_3 in table 7) and up to the 17.65 eV range, a wide and weak band is observed with numerous weak structures. A few of them could be regularly ordered in the 16.447-16.867 eV range (see table 7). They seem to involve a long and regular sequence of up to seven quanta of one vibrational mode with ω_i = 621 ± 24 cm^{-1} (77 ± 3 meV). By plotting ΔG_v versus the vibrational quantum number v, a strong anharmonicity coefficient $\omega_i x_i$ = 20 ± 3 cm^{-1} (2.5 ± 0.4 meV) is determined with a 0.94 correlation coefficient (see figure 8(a)).

Within the C_{2v} point group, the $\tilde{D}^2A_2$ state is a transition state, i.e. shows one imaginary wavenumber (table 4). This result has to be related to the fact that for the $\tilde{D}^2A_2$ state, within the C_{2v} point group at the QCISD level, the stationary point turns out to be a saddle point [23]. This state is also shown to cross both the $\tilde{B}^2A_1$ and $\tilde{C}^2B_2$ states [23]. The experimental value of 621 cm^{-1} lies between the calculated wavenumbers with $\omega_4(a_1)$ = 840 cm^{-1} or $\omega_5(a_1)$ = 460 cirr[1] as symmetry allowed transitions. These wavenumbers are associated with modes involving either C-F stretching or F-C-F bending. The imaginary frequency calculated for the $\tilde{D}^2A_2$ transition state is related to an antisymmetric C-F stretching. It might be assumed that the motion along this coordinate would lead to a structure where the C-F bonds have changed antisymmetrically, and that the observed frequency of 621 cm^{-1} could describe a less energetic C-F stretching for a longer C-F bond.

Above 16.924 eV (IE_4 in table 7) and up to 17.65 eV, a less regular sequence of very weak structures is observed. Energy intervals ranging from 57 to 72 meV are observed. The shape and intensity suggest the existence of (i) a new electronic state of the ion or (ii) the perturbation of the $\tilde{D}^2A_2$ state. From earlier quantum chemical calculations [2,3,23], the first excited state of the ion above the $\tilde{D}^2A_2$ state is the $\tilde{E}^2A_1$ state calculated at 18.25-18.49 eV [2, 3] or 18.33-18.70 eV [23] at different computational levels. Therefore, the structure observed in the 16.9-17.6 eV range is suggested to belong to the same but perturbed $\tilde{D}^2A_2$ state.

5.1.4. The fourth PES band: the $\tilde{E}^2A_1$ and $\tilde{F}^2B_1$ states (see figure 7(d)).

The PE band extending from 17.8 to 19.2 eV exhibits a well-defined vibrational structure giving rise to a very well-structured Δ plot shown in figure 7(d). The energy position of the features is listed in table 8. The adiabatic IE could only be estimated. By linear extrapolation of the low-energy side of this band, an IE_{ad} = 17.71 eV is obtained. A likely more accurate value is determined from the first peak in figure 7(d) at 17.835 eV (IE_1 in table 8). The vertical value IE_{vert} = 18.157 eV is measured. This latter value is in good agreement with that reported by Lake and Thompson at 18.22 eV.

This vertical IE should be compared to the results of quantum chemical calculations of the vertical ionization from the $7a_1$ and the $1b_1$ orbitals. They were computed at 17.47-18.49 and 16.96-18.71 eV, respectively, depending on the calculation levels [2, 3]. In our earlier work [23], the corresponding vertical IEs were calculated at 18.33-18.70 and 18.31-18.79 eV. On the basis of the vibrational analysis, the ionization from the $1b_1$ (see figure 5(f)) could have its onset at 18.985 eV (IE_2 in table 8).

Figure 8. *ΔG_v-versus-v plots for the $\tilde{D}^2A_2$ (a) and $\tilde{E}^2A_1$ (b) states of 1,1-$C_2H_2F_2^+$: the straight lines represent the least-squares fittings and the derived quantities are inserted.*

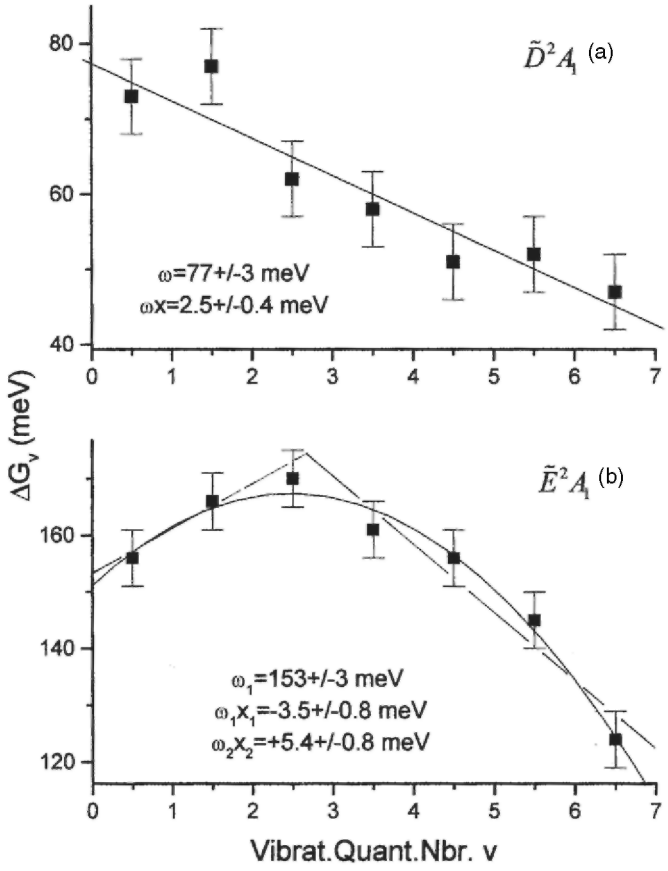

In the energy range of 17.7-19.3 eV, a very well-resolved vibrational structure is observed in the Δ plot (see figure 7(d)). An attempt to classify these structures is shown in table 8. A first progression consists of eight peaks with a very regular bell-shaped intensity distribution. Plotting the intervals ΔG_v versus the vibrational quantum number v, the diagram shown in figure 8(b) is obtained. A three-parameter polynomial fits the experimental points with a correlation coefficient of 0.98. Such a behaviour could be explained by an inversion of the sign of the anharmonicity. Fitting separately the two branches to a linear function of v leads to (i) a value of $hc\omega$ = 153 ± 3 meV (1234 ± 24 cm^{-1}) and (ii) two quite different anharmonicity values, i.e. $\omega|X|$ = -3.5 ± 0.8 meV (28 ± 6 cm^{-1}) and $\omega_2\chi_2$ = +5.4 ± 0.8 meV (44 ± 6 cm^{-1}). This inversion might be linked to a perturbation of the potential energy surface of the $\tilde{E}^2A_1$ state. Furthermore, from 18.157 to 18.985 eV, each of these vibrations is combined with a wavenumber of 597 ± 32 cm^{-1} (74 ± 4 meV).

The wavenumber of 1234 cm^{-1} obtained in this work is in good agreement with the value reported by Lake and Thompson [1] who measured 1270 cm^{-1} in the 18.22 eV PE band. However, no assignment is proposed by these authors.

No vibrational wavenumbers could be obtained at the B3LYP level for the $\tilde{E}^2A_1$ state and only an attempt for a reasonable assignment can be proposed. The ionized $7a_1$ orbital (see figure 5(g)) has a bonding character on the C = C, F-F and H-H bonds. The comparison of the wavenumber of 1234 cm^{-1} with the values listed in tables 4 and 5 would point to (i) the C = C stretching $\nu_2(a_1)$ motion with 1367-1795 cm^{-1} and even more to (ii) the H-C-H bending motion $\nu_3(a_1)$ whose predicted value oscillates between 1080-1438 crrr[1]. In the neutral molecule, these a_1 vibrational modes are characterized by ω_2 = 1730 cm^{-1} and ω_3 = 1354 cm^{-1} as measured by infrared and Raman spectroscopy [15] and predicted at 1747 and 1375 cm^{-1} [15] or at 1798 and 1421 cm^{-1} in this work (see table 3).

The transitions corresponding to the wavenumber of 597 ± 32 cm^{-1} are fairly strong, i.e. allowed transitions. This value could be compared to the wavenumber associated with the $\nu_5(a_1)$ mode characterized by a

wavenumber spread 460-573 cm^{-1} at the B3LYP level for the neutral and ionized molecule. It should involve the F-C-F bending vibration.

Above 18.9 eV, the Δ plot shows a slight increase of the intensity and a series of well-resolved weak peaks extends to 19.4 eV. This energy region very likely corresponds, at least partially, to the $\tilde{F}^2B_1$ ($1b_1^{-1}$) state of 1,1-$C_2H_2F_2^+$. The vibrational structure consists of intervals of 59 ± 5 meV (476 ± 40 cm^{-1}) between 19.058-19.230 eV and 19.317-19.441 eV. This wavenumber is rather close to ω_5 = 460 or 448 cm^{-1} [23] (see table 4) predicted for the $\tilde{D}^2A_2$ ionic state and could be, therefore, a probable assignment. The removal of one electron from the $1b_1$ orbital (see figure 5(f)) is expected to lead to the excitation of a normal mode involving the F-C-F bending.

Table 8. *Energy (eV) in the HeI-PES and TPES and assignments for the structures observed in the fourth band corresponding to the 1,1-$C_2H_2F_2^+$($\tilde{E}^2A_1$,$\tilde{F}^2B_1$) state: (0,0) means the vibrationless level.*

HeI-PES	TPES	Assignments
_	17.634	na
17.763	-	na
17.835	17.825	**$IE_1(\tilde{E}(0,0))$**[a]
17.929	17.935	na
17.991	17.985	**$IE_1+\nu_A$**
18.084	18.085	na
18.157	18.155	**$IE_1+2\nu_A$**
18.234	18.225	$IE_1+2\nu_A+\nu_B$
18.327	18.325	**$IE_1+3\nu_A$**
18.405	18.405	$IE_1+3\nu_A+\nu_B$
18.488	18.475	**$IE_1+4\nu_A$**
18.555	18.575	$IE_1+4\nu_A+\nu_B$
18.644	18.645	**$IE_1+5\nu_A$**
18.721	18.715	$IE_1+5\nu_A+\nu_B$
18.789	-	**$IE_1+6\nu_A$**
18.861	-	$IE_1+6\nu_A+\nu_B$
18.913	-	$IE_1+7\nu_A(+\nu_B)$
18.985	18.985	**$IE_2(\tilde{F}(0,0))$**[a]
19.058	19.065	$IE_2+\nu_c$
19.110	-	$IE_2+2\nu_c$
19.167	-	$IE_2+3\nu_c$
19.230	19.225	$IE_2+4\nu_c$
19.317	19.315	na[b]
19.379	19.385	na[b]
19.441	19.445	na[b]

[a] For the discussion, see section 5.1.4.
[b] For the explanation, see section 5.1.4.

5.1.5. The fifth PES band: the $\tilde{G}^2B_2$ state (see figure 7(e)).

The fifth band starting near 19.4 eV clearly shows a well-defined vibrational structure near 20 eV. Its Δ plot is displayed in figure 7(e) and the energy positions of the observed features are listed in table 9.

The energy covered by this band corresponds to the $\tilde{G}^2B_2$ ionic state of 1,1-$C_2H_2F_2^+$. The vertical IE of this state is predicted to be at 19.88-20.25 eV [23] or 17.83-19.89 eV [2, 3] depending on the calculation levels. These values have to be compared with the experimental IE_{vert} = 19.736 eV determined from the PES.

The Δ plot of this band (see figure 7(e)) is obviously divided in two very distinct parts consisting of (i) a bell-shaped intensity distribution between 19.483 eV (IE_1 in table 9) and 19.907 eV and (ii) a regularly decreasing intensity between 20.006 eV (IE_2 in table 9) and 20.627 eV. Their vibrational analysis also shows quite different results: (i) a low average energy interval of 86 ± 7 meV (694 ± 50 cm^{-1}) and (ii) a combination of energy intervals of 190 ± 10 meV (1540 ± 80 cm^{-1}) with 60 ± 6 meV (480 ± 48 cm^{-1}), respectively. This

observation should correspond to a strong perturbation of this ionic state through, e.g., an avoided crossing or a conical intersection.

Figure 9. *Δ plot of the TPES in the 17-22 eV photon energy region enhancing the vibrational structure in the $\tilde{E}^2A_1$-$\tilde{H}^2A_1$ bands.*

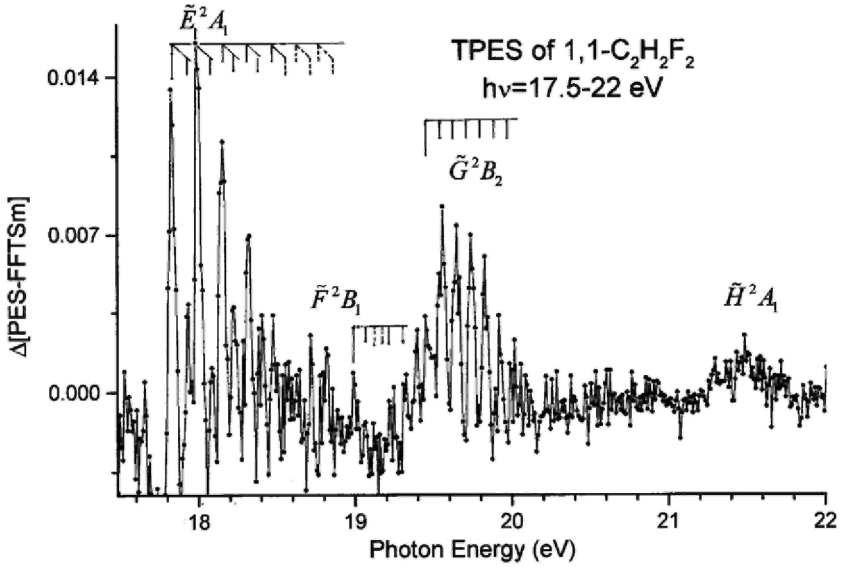

Table 9. *Energy (eV) in the HeI-PES and TPES and assignments for the structures observed in the fourth band corresponding to the 1,1-$C_2H_2F_2^+$($\tilde{G}^2B_2$) state: (0,0) means the vibrationless level.*

HeI-PES	TPES	Assignments
19.483	_	**IE_1**
19.560	19.555	$IE_1+\nu_A$
19.643	19.645	$IE_1+2\nu_A$
19.736	19.735	$IE_1+3\nu_A$
19.819	19.825	$IE_1+4\nu_A$
19.907	19.915	$IE_1+5\nu_A$
20.006	20.015	**IE_2**
20.058	-	$IE_2+\nu_C$
20.114	(20.105)[a]	$IE_2+2\nu_C$
20.198	(20.215)[a]	**$IE_2+\nu_B$**
20.260	(20.285)[a]	$IE_2+\nu_B+\nu_C$
20.322	-	$IE_2+\nu_B+2\nu_C$
20.374	(20.395)[a]	**$IE_2+2\nu_B$**
20.441	-	$IE_2+2\nu_B+\nu_C$
20.508	(20.525)[a]	$IE_2+2\nu_B+2\nu_C$
20.570	-	**$IE_2+3\nu_B$**
20.622	(20.615)[a]	$IE_2+\nu_B+\nu_C$

[a] Data in parentheses are obtained from smoothed data (see the text).

5.2. The TPE and CIS spectra

5.2.1. The TPE spectrum of 1,1-$C_2H_2F_2$ (figures 1(a) and 9).

The TPES of 1,1-$C_2H_2F_2$ recorded between 8 and 28 eV is shown in figure 1(a). Except for the relative intensities of the bands, the TPES reproduces almost the HeI-PES shown in figure 1(b). Normalizing the intensities of the first TPES band to those of the HeI-PES band of the ground ionic state, the most enhanced part of the TPE spectrum is in the 13 eV photon energy range where the intensity is increased by a factor 9. The strongest TPES bands in the 14-17 eV range are enhanced by factors of 6 and 4, respectively. In the 17-21 eV

range, the intensity ratio is about 2. Furthermore, data are obtained above the 21.22 eV energy boundary. Band maxima are detected at 21.48 and 24.14 eV, successively.

The large discrepancy of the ionization cross-sections between the HeI and TPE spectra can only be interpreted with the help of both the CIS spectra and the PAS [14]. Both are shown in figure 2 in the 10-25 eV photon energy range. Five spectral regions (labelled a-e in figure 2(b)) are related to energy ranges where Rydberg transitions have been observed and the details of their assignment have been discussed in an earlier report [14].

The only data available about the PES of 1,1-$C_2H_2F_2$ above the 21.22 eV limit are those obtained by Bieri *et al* [2] using the HeII line at 30.4 nm. These authors report vertical IEs at 21.5 and 25.2 eV. A closer examination of their spectrum clearly shows the presence of a PES band with a maximum at about 23.9 eV, i.e. just below the He ionization line at 24.587 eV. As shown in figure 1(a) the last TPES band is spread between 22.4 and 25.7 eV. Within the detection limits no additional band is detected up to 28 eV photon energy.

To check the presence of a vibrational structure in the TPES bands above 18 eV photon energy, the subtraction method has been applied to this part of the spectrum (see section 2.2). The result is shown in figure 9 between 17.5 and 22 eV photon energy. The signal-to-noise ratio is less favourable than in the case of the HeI-PES (see figures 7(d) and (e) for comparison). However, the major progressions are unambiguously identified for, e.g., the $\tilde{E}^2A_1$ and the $\tilde{G}2B_2$ states. The energy positions and the intensity distributions are in good agreement with the PES data. After a slight smoothing of the Δ plot, several additional features could be identified (in parentheses in table 9). Owing to this unfavourable signal-to-noise ratio, no vibrational structure could be identified in the 20-22 eV photon energy range. At most an adiabatic IE at 21.2 eV could be measured for the TPES band at 21.5 eV.

Ab initio calculations at different levels have been applied for the assignment of the high-energy PES bands [2, 3, 23]. Bieri *et al* [2, 3] calculated vertical IE values of 20.4-21.8 eV and 25.4-27.1 eV for the $\tilde{H}^2A_1$ (oar^1) and the $\tilde{I}^2A_1$ ($5a_1^{-1}$) ionic states, respectively. In our earlier work on 1,1-$C_2H_2F_2$[23], only $IE_{vert}(\tilde{H}^2A_1)$ = 21.82-22.26 eV has been calculated.

Below 21.22 eV, the TPES of 1,1-$C_2H_2F_2$ shows many features in the five bands, in marked contrast with the TPES of C_2H_3F [8]. The position in energy of these structures and their assignment as discussed in detail in section 5.1 are listed in tables 6-9. The largest difference between the TPES and HeI-PES, as concerning the intensities and the observed energy positions, is observed between 11.7 and 13.5 eV photon energy. As discussed in section 5.1.1, the extended vibrational structure observed in the HeI-PES is assigned to autoionizing transitions from one neutral (Rydberg) state to the upper vibrational levels of the 1,1-$C_2H_2F_2$ ($\tilde{X}^2B_1$) ionic state. In the TPES the same explanation should hold but in this case the population of the upper levels of the 1,1-$C_2H_2F_2$ ($\tilde{X}^2B_1$) state occurs by resonant autoionizing transitions from successive vibronic Rydberg states.

5.2.2. The CIS photoelectron spectra of 1,1-$C_2H_2F_2^+$ (figures 2(a) and 3).

The CIS spectrum extending over 10 eV photon energy has been recorded for each individual ionic state at its corresponding vertical IE for the $\tilde{X}^2B_1$ state to the $\tilde{H}^2A_1$ state (see figure 2(a)).

It is very noteworthy that the CIS spectra of almost all excited ionic states show the same profile: the cross-section decreases exponentially over about 2 eV without any structure and then levels off to an approximately common limited. This suggests that the relative intensity differences of the successive PE bands between the TPES and HeI-PES have been mainly assigned to resonant or nearly resonant autoionization. Only the $\tilde{D}^2A_2$ state behaves quite differently: the decrease extends over about 4 eV and the cross-section markedly increases above 22 eV photon energy. These observations in the CIS spectra of the 1,1-$C_2H_2F_2^+$ are notably different from those of $C_2H_3F^+$ [8] where clearly the individual contribution of the successive Rydberg states could be identified.

Vibrationally resolved CIS spectra have been recorded between 10-20 eV for the $\tilde{X}^2B_1$ ground ionic state and are displayed in figure 3 for the ν_2 vibrational motion between ν = 0-3. A CIS spectrum has also been recorded for 12.9 eV, i.e. in the energy range of the upper vibrational levels of the $\tilde{X}^2B_1$ observed in both the TPES and the HeI-PES (see figure 1 (b)), but with very low intensity in the latter. Contrary to the observations made for $C_2H_3F^+$ [8], vibrational specificity is observed within the electronic ground state of the ion.

Obviously, the CIS spectrum for $\tilde{X}^2B_1$ (v = 0) is quite different from those of the $\tilde{X}^2B_1$(v =1, 2 and 3) levels. Even more remarkable is the CIS spectrum recorded at 12.9 eV. The latter is quite similar to that of the $\tilde{D}^2A_2$ state, but decreases asymptotically to zero above 16 eV photon energy. Obviously, resonant autoionization of Rydberg states of regions a and b in the PAS (see figure 2(b)) contribute substantially to the population of the high vibrational levels of the $\tilde{X}^2B_1$ ionic state. For the CIS of the $\tilde{X}^2B_1$ (v = 0) highly excited vibronic states between 10-12 eV populate the ionic state as do to a lesser extent Rydberg states of the b-e PAS region (see figure 2(b)).

In contrast, for the $\tilde{X}^2B_1$ (v = 1-3) the autoionizing contribution of the b-e PAS region dominates the CIS spectra. It is noteworthy that the cross-sections increase steadily starting around 16 eV and this increase most probably extends above 20 eV. This indicates that autoionization contributes to the HeI-PES (21.22 eV) and could be responsible for the extended vibrational structure detected in the 12-14 eV region.

6. Conclusions

he HeI photoelectron, threshold photoelectron and constant ion state spectroscopies have been applied for the detailed investigation of the photoionization of 1,1-$C_2H_2F_2$.. The application of a subtraction method to the spectra allowed us to analyse in detail the abundant vibrational structure observed in most of the PES and TPES bands. *Ab initio* quantum chemical calculations applied to the 1,1-$C_2H_2F_2^+$ cation provided the essential reference data for the assignment of the numerous structures present in the spectra. Although of quite weak intensity, an extensive vibrational structure has been observed between the $\tilde{X}^2B_1$ and $\tilde{A}^2B_2$ ionic states. It has been assigned to the population of the $\tilde{X}^2B_1$ state through autoinization of a Rydberg state resonant with the HeI-54.8 nm resonance line. Several details observed in various PE bands could be linked to the appearance of several fragment ions as well as to the existence of conical intersections and/or avoided crossings identified by the theoretical calculations [23] and recent experimental observations [25].

Acknowledgments

We are indebted to the University of Liège and the Fonds de la Recherche Fondamentale Collective (FRFC) for financial support. RL and BL gratefully acknowledge the European Community for its support through its TMR (contract EU-HPRI-1999CT-00028) and 13 (contract R II 3 CT-2004-506008). DD's contribution was supported by the Belgian programme on Interuniversity Attraction Poles of the Belgian Science Policy (IAP n°P6/19).

References

[1] Lake R F and Thompson H 1970 *Proc. R. Soc. Lond.* A **315** 323
[2] Bieri G, Asbrink L and Von Niessen W 1981 *J. Electr. Spectrosc. Rel. Phenom.* **23** 281
[3] Bieri G, Von Niessen W, Asbrink L and Svensson A 1981 *Chem. Phys.* **60** 61
[4] Heaton M M and El-Talbi M R 1986 *J. Chem. Phys.* **85** 7198
[5] Pradie N A and Linnert H V 2007 *J. Phys. Chem.* A **111** 4836
[6] Reinke D, Krässig R and Baumgärtel H 1973 *Z. Naturf.* **28a** 1021
[7] Kaufel R 1985 *PhD Thesis* Freie Universität Berlin
[8] Locht R, Leyh B, Dehareng D, Hottmann K and Baumgärtel H 2010 *J. Phys.* B **43** 015102
[9] Locht R, Leyh B, Hottmann K and Baumgärtel H 1997 *Chem. Phys.* **220** 217
[10] Hoxha A, Locht R, Leyh B, Dehareng D, Hottmann K, Jochims H W and Baumgärtel H 2000 *Chem. Phys.* **256** 239
[11] Reichardt G, Noll T, Packe I, Rotter P, Schmidt J-S and Gudat W 2001 *Nucl. Instrum. Methods* A **467-468** 458
[12] Locht R, Caprace G and Momigny J 1984 *Chem. Phys. Lett.* **111** 560
[13] Locht R, Leyh B, Denzer W, Hagenow G and Baumgârtel H 1991 *Chem. Phys.* **155** 407
[14] Locht R and Leyh B 2012 *Chem. Phys.* submitted [15] Jiang H, Appadoo D, Robertson E and McNaughton D 2002 *J. Comput. Chem.* **23** 1220
[16] Frisch M J *et al* 2003 *GAUSSIAN 03, Revision B.04* (Pittsburgh, PA: Gaussian)
[17] Pople J A, Head-Gordon M and Raghavachari K 1987 *J. Chem. Phys.* **87** 5968
[18] Parr R G and Yang W 1989 *Density Functional Theory of Atoms and Molecules* (New York: Oxford University Press)
[19] Becke A D 1993 *J. Chem. Phys.* **98** 5648
[20] Hegarty D and Robb M A 1979 *Mol. Phys.* **38** 1795
[21] Eade R H E and Robb M A 1981 *Chem. Phys. Lett.* **83** 362
[22] Bernardi F, Bottini A, McDougall J J W, Robb M A and Schlegel H B 1984 *Faraday Symp. Chem. Soc.* **19** 137
[23] Gridelet E, Dehareng D, Locht R, Lorquet A J, Lorquet J C and Leyh B 2005 *J. Phys. Chem.* A **109** 8225
[24] Natalis P 1973 *Mém. Cl. Sc. Acad. R. Belg.* **XLI** (1) 61
[25] Harvey J, Bödi A, Tuckett R.P and Sztaray B 2012 *Phys. Chem. Chem. Phys.* **14** 3935